Dalton Transactions

Accepted Manuscript

ROYAL SOCIETY OF CHEMISTRY

www.rsc.org/dalton

Calcium and heterometallic manganese-calcium complexes supported by tripodal pyridine-carboxylate ligands: structural, EPR and theoretical investigations

Bertrand Gerey,[a] Marcello Gennari,[a] Eric Gouré,[a] Jacques Pécaut,[b] Allan Blackman,[c] Dimitrios A. Pantazis,[d] Frank Neese,[d] Florian Molton,[a] Jérôme Fortage,[a] Carole Duboc,[a] and Marie-Noëlle Collomb[a*]

[a]Univ. Grenoble Alpes, DCM UMR 5250, F-38000 Grenoble, France
CNRS, DCM UMR 5250, F-38000 Grenoble, France

[b]Univ. Grenoble Alpes, INAC-SCIB, F-38000 Grenoble, France
CEA, INAC-SCIB, Reconnaissance Ionique et Chimie de Coordination, F-38000 Grenoble, France

[c]School of Applied Sciences, Auckland University of Technology, Private Bag 92006, Auckland 1142, New Zealand

[d]Max-Planck-Institut für Chemische Energie Konversion, Stiftstrasse 34-36, D-45470 Mülheim an der Ruhr, Germany

Abstract

Carboxylate-bridged Mn(II)-Ca(II) complexes are potentially relevant for mimicking the first stages of the Oxygen-Evolving Complex (OEC) assembly process. Here, we report on new homonuclear Ca(II) and heteronuclear Mn(II)-Ca(II) complexes with carboxylate-functionalized tripodal tris(2-pyridylmethyl)amine ligands, the heptadentate H_3tpaa, previously reported, and the new hexadentate H_2tpada, containing respectively three and two carboxylate units. The mononuclear [Ca(Htpaa)(OH_2)] (**Ca$_1$**) and dinuclear [Ca(tpada)(OH_2)$_2$]$_2$ (**Ca$_2$**) calcium complexes, as well as the tetranuclear [{Mn(tpaa)}$_2${Ca(OH_2)$_5$(μ-OH_2)}$_2$][Mn(tpaa)]$_2$ (**Mn$_2$Ca$_2$·2Mn**) and dinuclear [Mn(tpada)ClCa(OH_2)$_{2.67}$(MeOH)$_{2.33}$]Cl (**MnCa**) heterometallic species have been structurally characterized; the syntheses of **Ca$_1$** and **Mn$_2$Ca$_2$·2Mn** being previously reported by us (*Inorg. Chem. 2015, 54, 1283*). The Mn(II) and Ca(II) are linked by two $\mu_{1,1}$-bridging carboxylates in **MnCa**, while only one $\mu_{1,3}$-carboxylate bridge connects each Ca^{2+} ion to each Mn(II) in **Mn$_2$Ca$_2$**. A variable number of water molecules (n = 1 to 7) are coordinated to Ca in all complexes, most of them being involved in hydrogen-bond networks, in analogy to what occurs in the photosystem II. All donor atoms of the $tpaa^{3-}$ and $tpada^{2-}$ ligands are coordinate to the Mn^{2+} ions, despite the unusually long distance between the Mn^{2+} ion and the tertiary amine imposed by the constrain nature of the ligands, as supported by theoretical calculations. Solid state EPR spectroscopy, in combination with DFT calculations, have also shown that the Ca^{2+} ion has an effect on the electronic parameters (zero field splitting) of the linked Mn(II) in the case of **MnCa** ($\mu_{1,1}$-carboxylate bridges). In **Mn$_2$Ca$_2$** ($\mu_{1,3}$-carboxylate bridge) the Ca^{2+} ion induces only slight structural changes in the Mn coordination sphere.

Introduction

The catalytic oxidation of water into dioxygen is performed by the Oxygen – Evolving – Center (OEC) of photosystem II (PSII), an oxygen-bridged cluster of four manganese and one calcium ions (Mn_4CaO_x) stabilized by carboxylate ligands.[1-3] Recent X-ray diffraction (XRD) and X-ray free electron laser (XFEL) studies[4, 5] have revealed that, in its native state, the OEC consists of a $[Mn_3CaO_3(OH)]$ cubanoid linked to a fourth dangling manganese ion through one oxo and the hydroxo of the cubane. Four water molecules directly coordinated to the cluster (two to the Ca^{2+} ion and the other to the outer manganese) may act as substrates for dioxygen formation.[6-9] The extensive hydrogen-bond network around the cluster involving these water molecules supports Proton Coupled Electron Transfer (PCET) pathways for water oxidation. Only high oxidation states of manganese are believed to be involved in the catalytic cycle of the OEC, the more reduced intermediate being likely assigned to a $Mn^{III}_3Mn^{IV}$ state.[4, 10] How the O-O bond is formed, the precise site of its formation and the specific role of the essential Ca^{2+} ion, are currently the most debated aspects regarding the water oxidation mechanism.[11-14] Many oxo/acetato-bridged polynuclear manganese complexes have been synthesized[15-21] in order to improve the understanding on the structural, spectroscopic properties and function of the OEC. By contrast, the synthesis and investigation of hetero-nuclear manganese-calcium complexes are still largely unexplored with less than twenty examples of synthetic clusters[22-36] or polymers[37-40] isolated to date, incorporating Mn in the (II-IV) oxidation states. Amongst these compounds, if the two oxo-bridged cubane clusters, $[Mn^{IV}_3CaO_4]^{6+}$ and $[Mn^{IV}_3Ca_2O_4]^{8+}$ isolated in 2011 by the groups of Agapie[33-35] and Christou[24], have emerged as the best structural models of the OEC cubanoid unit, the first structural mimic of the full site of the OEC, a cubane $Mn_3^{IV}Mn^{III}CaO_4$ linked to a dangling Mn^{III} via one oxo bridge of the cubane, has just been reported by Zhang et al.[41]

Even if the OEC contains Mn ions in high oxidation states (like the Agapie's, Christou's and Zhang's models), it is interesting to note that the OEC is assembled via the so-called "photoactivation" process, initiating from Mn^{2+} in the presence of the cofactor-depleted PSII, Ca^{2+}, chlorides, water and light.[3, 42, 43] Photoactivation occurs naturally during biogenesis or repair of PSII centers. Repair of PSII is steadily required as its structure is partially damaged under continuous illumination, so that the inorganic OEC catalyst needs to be regularly replaced and reassembled (every 30 min at full solar flux). Calcium is essential for this photoactivation process: in the absence of Ca^{2+} an excessive incorporation of Mn ions has been reported, leading to the complete inhibition of O_2 evolution activity.[44] The presence of

competing Ca^{2+} ions is thus proposed to control the coordination properties of manganese and the oligomerisation process. In the early steps of photoactivation, labile Mn^{2+} and Ca^{2+} ions are proposed to assemble in bridged $Mn^{2+/3+}$-Ca^{2+} species, the geometry of which allows for gradual hydration and photooxidation to the final OEC cluster.[3, 42] In this respect, Agapie proposed the association of Ca^{2+} to a trimanganese(II) core via $\mu_{1,3}$ acetate bridges as an intermediate in the formation of the heterometallic $[Mn_3CaO_4]$ cubane reported by his group. This offers insights into a potential mechanism of OEC assembly.[33] In this context, the development of new $Mn^{2+/3+}$-Ca^{2+}complexes bridged by carboxylate units is relevant for mimicking the first stages of the OEC assembly process since the number of such heterobimetallic complexes is still limited to a few examples.[25, 26, 37, 38, 40] Such compounds are required as further benchmarks, ideally to fully understand how the Mn/Ca composition, nuclearity and relative arrangement of metals in these species can be controlled. In most of the reported systems, the synthetic route employed is based on self-assembly from Mn and Ca salts in the presence of carboxylate-free chelating ligands, with carboxylates that are added as ancillary bridging ligands. The less explored strategy adopted in this work is based on the use of multidentate ligands that incorporate carboxylate functions in the ligand framework. In particular, two tripodal tris(2-pyridylmethyl)amine derivatives functionalized with three and two carboxylate moieties are used in this present study: the previously reported heptadentate N'N3O3 donor H_3tpaa ligand[45] and the new hexadentate N'N3O2 donor H_2tpada ligand (both depicted in Scheme 1).

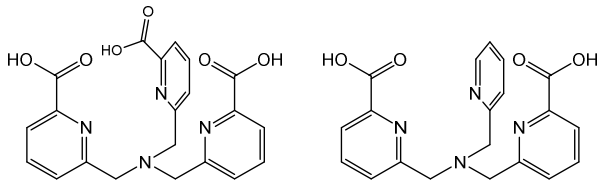

H_3tpaa H_2tpada

Scheme 1. H_3tpaa and H_2tpada ligands.

We have explored the molecular architectures arising by assembling these ligands in presence of Ca^{2+} ions and also in combination with Mn^{2+} ions. As a result, homonuclear Ca and heteronuclear carboxylate-bridged Mn(II)-Ca complexes with different nuclearities were obtained and structurally characterized: $[Ca(Htpaa)(OH_2)]$ (**Ca_1**), $[Ca(tpada)(OH_2)_2]_2$ (**Ca_2**), $[\{Mn(tpaa)\}_2\{Ca(OH_2)_5(\mu\text{-}OH_2)\}_2][Mn(tpaa)]_2$ (**Mn_2Ca_2·2Mn**) and $[Mn(tpada)ClCa(OH_2)_{2.67}(MeOH)_{2.33}]Cl$ (**MnCa**). Among these compounds, the **Ca_1** and **Mn_2Ca_2·2Mn** complexes having 8-coordinated Ca centers have been the subject of a recent investigation by Ca K-edge X-ray absorption (XAS) along with Agapie's 6 and 7-coordinated

heterometallic MnCa clusters[33, 35] and Ca inorganic compounds.[46] In the present study, we discuss the synthesis and X-Ray structures of all the previously listed Ca and carboxylate-bridged Mn(II)-Ca complexes with the tpaa and tpada ligands. In **MnCa** and **Mn_2Ca_2·2Mn**, the distribution of the bonding around the Mn^{2+} ions in **MnCa** and **Mn_2Ca_2·2Mn** complexes has been also investigated by DFT calculations in order to firmly establish the coordination of the tertiary amine of the ligands to the Mn^{2+} ions in these complexes. In addition, EPR spectroscopy, in combination with theoretical calculations, has allowed us to study how the calcium can influence the electronic structure of the Mn^{2+} ion in these heteronuclear compounds.

Results and discussion

Synthesis and coordination properties of the ligands

H_3tpaa was synthesized according to a procedure published by the group of Mazzanti.[45] The coordination properties of this ligand with lanthanide, lead and calcium ions have been investigated by the same group.[47, 48] Here, a similar synthetic strategy has been adopted for the preparation of the new H_2tpada ligand. This ligand was obtained by hydrolysis of Me_2tpada, which was prepared by nucleophilic substitution of 2-bromomethyl-6-pyridine carboxylic acid methyl ester with 2-picolylamine (half an equivalent), with a total yield of 34% (Scheme 2). H_2tpada was isolated in a HPF_6-salt form, in order to avoid the co-precipitation of lithium salts with the ligand. Whereas H_3tpaa can act as an heptadentate NN'_3O_3 ligand (N atom from the tertiary amine, N' atoms from the pyridyl groups and O atoms from carboxylates), H_2tpada is potentially hexadentate NN'_3O_2, as it contains only two pyridyl groups functionalized with carboxylic acids.

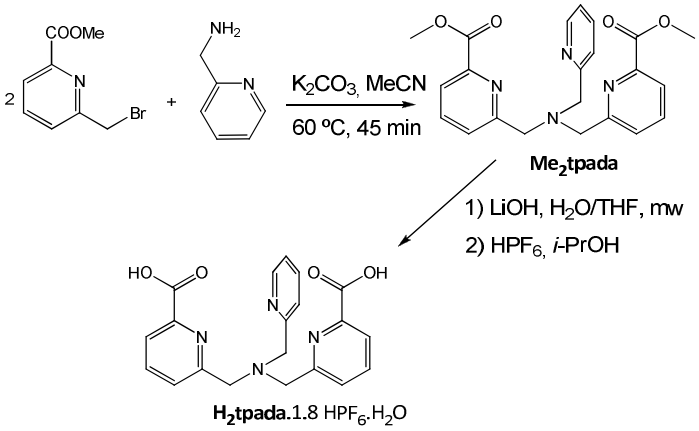

Scheme 2. Synthetic route for the H_2tpada ligand.

Synthesis and crystal structures of the complexes

As a general procedure for the synthesis of the Ca(II) and Mn(II)-Ca(II) complexes, the carboxylate units of the ligands were first deprotonated by addition of a base to a suspension of the ligand in water, leading to their dissolution. After addition of the appropriate metal salts, the complexes were then crystallized following the procedures depicted in Scheme 3.

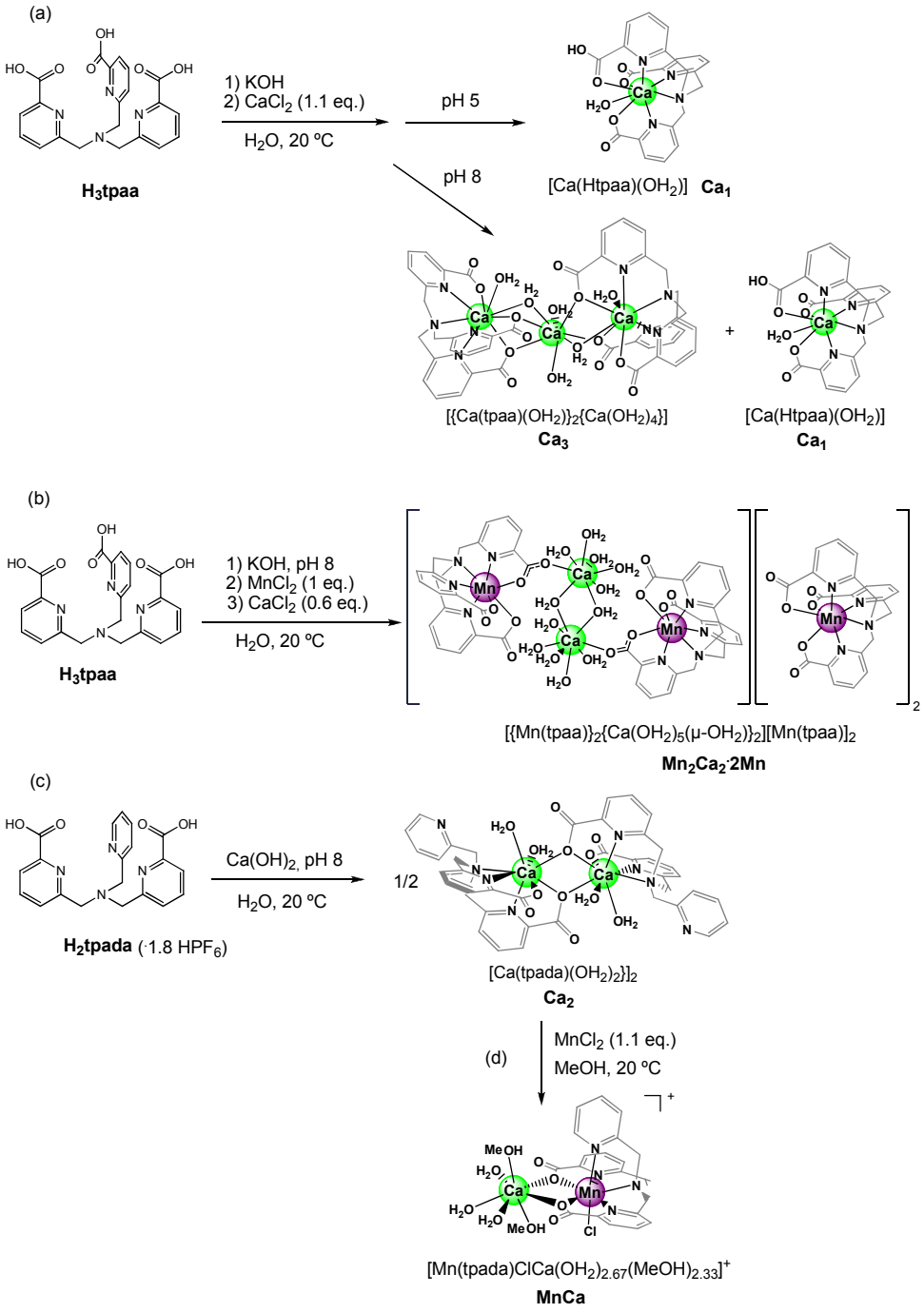

Scheme 3. Synthesis of the Ca and Mn-Ca complexes.

As a result, we have isolated and structurally characterized one mononuclear and one dinuclear neutral Ca complexes, $[Ca(Htpaa)(OH_2)]$ (**Ca$_1$**) and $[Ca(tpada)(OH_2)_2]_2$ (**Ca$_2$**), respectively, and two heteronuclear Mn-Ca complexes: $[\{Mn(tpaa)\}_2\{Ca(OH_2)_5(\mu\text{-}OH_2)\}_2][Mn(tpaa)]_2$ (**Mn$_2$Ca$_2$·2Mn**), containing a tetranuclear Mn_2Ca_2 cationic unit, and the dinuclear $[Mn(tpada)ClCa(OH_2)_{2.67}(MeOH)_{2.33}]Cl$ (**MnCa**). In these two latter compounds, the Mn^{2+} and the Ca^{2+} ions are bridged via μ-carboxylato units. Interestingly, the **MnCa** complex is the second example of a low nuclearity binuclear Mn-Ca complex. The first one isolated by the group of Borovik,[32] possessing an unprecedented Mn^{III}-(μ-OH)-Ca unit, has been also achieved from a tripodal ligand. The crystallographic data, selected bond distances and angles, and hydrogen bonds for the different complexes are summarized in Tables 1-2, S1-S11. The Ca^{2+} ions are eight-coordinated in both **Ca$_1$** and **Ca$_2$** complexes and in the **Mn$_2$Ca$_2$** unit, showing N_4O_4, N_3O_5 and O_8 coordination spheres, respectively. By contrast, a seven-coordinate Ca^{2+} with an O_7 coordination sphere is found in **MnCa**. The Mn^{2+} ions are also seven-coordinate (see below) with a N_4O_3 and N_4O_2Cl environment in **Mn$_2$Ca$_2$·2Mn** and **MnCa**, respectively. Interestingly, in all of these complexes, calcium coordinates aqua ligand(s) whose number varies from one to seven.

Complex $[Ca(Htpaa)(OH_2)]\cdot 4.5H_2O$ (Ca$_1$·4.5H$_2$O). The reaction of the tris(picolinate) ligand H_3tpaa with $CaCl_2$ at pH 8 in water leads, after slow evaporation of the solvent, to a mixture of colourless single crystals of the previously reported neutral trinuclear $[\{Ca(tpaa)(OH_2)\}_2\{Ca(OH_2)_4\}]$ (**Ca$_3$**)[48] and of the new mononuclear $[Ca(Htpaa)(OH_2)]\cdot 4.5H_2O$ (**Ca$_1$**·4.5H$_2$O) complexes (Scheme 3(a)).[46] In **Ca$_3$**, two symmetric anionic $\{Ca(tpaa)(OH_2)\}^-$ units are connected to a central cationic aquo complex $\{Ca(OH_2)_4\}^{2+}$ through bridging water molecules and carboxylates. We have found that it is possible to orient the synthesis towards the quantitative formation of **Ca$_1$**, which contains a monoprotonated $Htpaa^{2-}$ ligand (see below), by conducting the reaction at pH 5. Under these more acidic conditions, **Ca$_1$** precipitates in the reaction medium. Therefore, the pH value seems crucial for directing the process towards different nuclearities of the formed Ca species: at acidic pH the mononuclear $\{Ca(tpaa)(OH_2)\}^-$ unit is protonated to compensate its negative charge, whereas at higher pH the negative charge is preferably balanced by bridging $\{Ca(OH_2)_4\}^{2+}$ moieties affording the trinuclear **Ca$_3$**.

The structure of the mononuclear complex **Ca$_1$**·4.5H$_2$O consists of central Ca^{2+} ion coordinated to seven donor atoms of the heptadentate $Htpaa^{2-}$ ligand (one tertiary amine N atom, three pyridyl N atoms and three carboxylate O atoms) and a single aqua ligand (Figure

1). As is the case with many other 8-coordinate complexes, it is difficult to describe the coordination environment around the metal ion simply in terms of the three 'ideal' geometries, namely the trigonal dodecahedron, square antiprism or bicapped trigonal prism.[49] In this case, the geometry about the Ca^{2+} ion is best described as distorted trigonal dodecahedral; the ligand donor atoms O1, N1, N2, N11 and O11 form a very approximate plane containing the metal ion, while the two remaining ligand donor atoms N21 and O21, and the aqua ligand donor atom O31, lie above and below this plane, respectively.

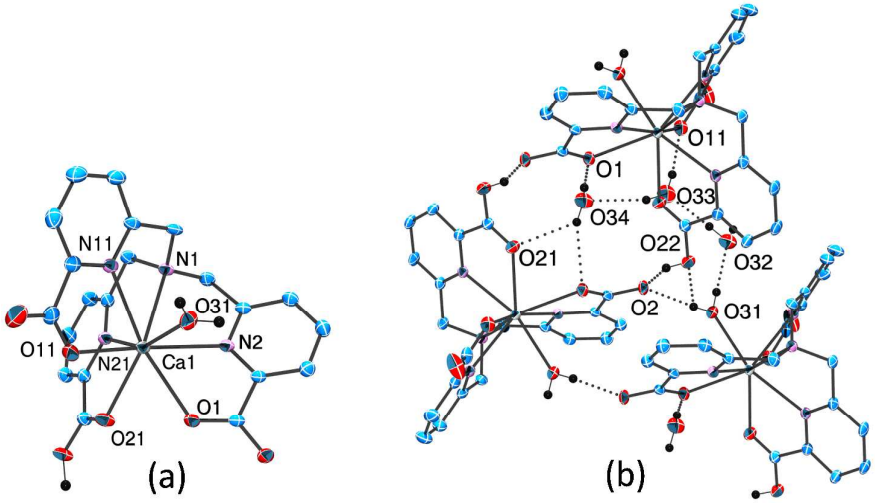

Figure 1. ORTEP drawings with thermal ellipsoids at 50% probability of the $\mathbf{Ca_1}\cdot 4.5H_2O$ complex; view of (a) the $\mathbf{Ca_1}$ unit and (b) the hydrogen bond network of complex $\mathbf{Ca_1}$ with three co-crystallized water molecules. Only relevant hydrogens are shown for clarity.

Charge consideration requires the $Htpaa^{2-}$ ligand to be monoprotonated. This is supported by the significantly longer C27-O22 bond distance (1.304(4) Å), and thus shorter C27-O21 bond distance (1.214(4) Å)) than those of the two other carboxylate C-O bonds (Table S2), as well as for those of all the other compounds discussed in this work (Tables S4, S7, S8 and S10). The Ca-N bond involving the tertiary N atom N(1) is significantly longer than the Ca-N_{py} ones while the Ca-O bond length of the aquo ligand of 2.401 Å is close to those of the carboxylato which range from 2.404 Å to 2.461Å (Table 1). Extensive hydrogen bonding interactions are present throughout the structure (Figure 1(b), Table S3); the carboxylate oxygen atoms hydrogen bind both to co-crystallized water molecules and to carboxylate O atoms of neighbouring molecules, while the coordinated aqua O atom, as well as being hydrogen-bonded to a water of crystallisation, also exhibits an intermolecular hydrogen bond to an adjacent carboxylate O atom (O2····O31 = 2.777(3) Å).

Table 1. Selected bond lengths (Å) and angles (deg) in complexes **Ca$_1$**·4.5H$_2$O and **Ca$_2$**·5.2H$_2$O.

Ca$_1$·4.5H$_2$O		**Ca$_2$**·5.2H$_2$O	
Ca(1)-N(1)$_{tert}$	2.741(2)	Ca(1)-N(1)$_{tert}$	2.7616(16)
Ca(1)-N(2)$_{pyr}$	2.547(3)	Ca(1)-N(2)$_{pyr}$	2.5355(16)
Ca(1)-N(11)$_{pyr}$	2.503(3)	Ca(1)-N(3)$_{pyr}$	2.5543(16)
Ca(1)-N(21)$_{pyr}$	2.581(2)		
Ca(1)-O(1)$_{COO-}$	2.454(2)	Ca(1)-O(3)$_{COO-}$	2.4253(14)
Ca(1)-O(11)$_{COO-}$	2.404(2)	Ca(1)-O(1)$_{\mu\text{-}COO-}$	2.4664(13)
Ca(1)-O(21)$_{COOH}$	2.461(2)	Ca(1)-O(1)#$_{\mu\text{-}COO-}$	2.4954(13)
Ca(1)-O(31)$_{H2O}$	2.401(2)	Ca(1)-O(11)$_{H2O}$	2.4273(15)
		Ca(1)-O(12)$_{H2O}$	2.4196(16)

 # = -x, -y, -z

Complex [Ca(tpada)(OH$_2$)$_2$]$_2$·5.2H$_2$O (Ca$_2$·5.2H$_2$O). This calcium complex was synthesized by reaction of H$_2$tpada with Ca(OH)$_2$ at pH 8 in water (Scheme 3(c)). The structure of **Ca$_2$**·5.2H$_2$O consists of dimeric units in which each Ca^{2+} ion is coordinated to a potentially hexadentate $tpada^{2-}$ ligand through the tertiary amine N atom, two pyridyl N atoms and two carboxylate O atoms, and to two aqua ligands (Figure 2). Coordination about each Ca^{2+} ion is completed by a single carboxylate O atom of a neighbouring {(Ca(tpada)} unit, which bridges the two Ca^{2+} ions in a $\mu_{1,1}$ fashion, thereby forming centrosymmetric dimeric units.

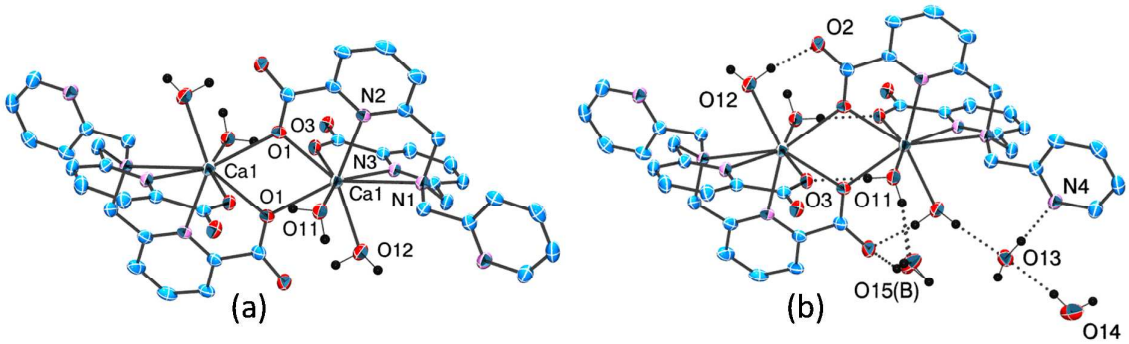

Figure 2. ORTEP drawing with thermal ellipsoids at 50% probability of the **Ca$_2$**·5.2H$_2$O complex; view of (a) the **Ca$_2$** unit and (b) the intramolecular hydrogen bond network of complex **Ca$_2$** and with 2.6 co-crystallized water molecules of the asymmetric unit. Only relevant hydrogens are shown for clarity.

The tpada ligand is hypodentate,[50, 51] with the unique pyridine ring remaining uncoordinated to the metal ion. Undoubtedly, this favors the coordination of exogenous ligands, like water molecules to Ca^{2+}, in order to complete the coordination sphere around the metal center. Also in this case the geometry about each 8-coordinate Ca^{2+} ion is best described as distorted trigonal dodecahedral; the metal ion is approximately coplanar with five donor atoms (one

tertiary N, one pyridyl N, one aqua O and two carboxylate O atoms), with, respectively, one aqua O and one chelating carboxylate O/pyridyl N pair of atoms occupying pseudo axial sites. As in **Ca_1**, the Ca-N bond involving the tertiary N atom N(1) is longer than the Ca-N_{py} ones (Tables 1, S4). Although there are three different types of O donor atom in the molecule (aqua, monodentate carboxylate, bridging $\mu_{1,1}$-carboxylate) there are only small differences in the Ca-O bond lengths, which range from 2.420 Å to 2.495 Å. The coordinated aquo-ligands are involved in hydrogen-bond interactions, both with adjacent carboxylates and with co-crystallized water molecules, as O(13) which is H-bonding with the dangling pyridine (Figure 2(b), Table S5). The overall structure is very similar to that obtained using the related pentadentate ligand $dpaea^{2-}$ (H_2dpaea = *N*,*N*-bis[(6-carboxypyridin-2-yl)-methyl]ethylamine), $[\{Ca(dpaea)(CH_3OH)(OH_2)\}_2]$,[48] except that in this previously isolated structure, the axial ligand is a molecule of methanol.

Complex $[\{Mn(tpaa)\}_2\{Ca(OH_2)_5(\mu\text{-}OH_2)\}_2][Mn(tpaa)]_2\cdot 25H_2O$ (**Mn_2Ca_2·2Mn**·25H_2O). The reaction of the tris(picolinate) ligand H_3tpaa with a mixture of $MnCl_2$ (1 eq.) and $CaCl_2$ (0.6 eq.) at pH 8 in water leads to **Mn_2Ca_2·2Mn**·25H_2O (Scheme 3(b)).[46] The same product crystallized when a larger amount of Ca^{2+} salt was employed ($CaCl_2$ or $Ca(OAc)_2$) (1 eq. *vs* H_3tpaa and Mn^{2+} salt instead of 0.6), attesting its thermodynamic stability. The structure of **Mn_2Ca_2·2Mn**·25H_2O consists of a centrosymmetric tetrametallic $[\{Mn(tpaa)\}_2\{Ca(OH_2)_5(\mu\text{-}OH_2)\}_2]^{2+}$ cation, in which two anionic $[Mn(tpaa)]^-$ moieties are bridged by a dimeric $[\{Ca(OH_2)_5(\mu\text{-}OH_2)\}_2]^{4+}$ unit via $\mu_{1,3}$-carboxylate, together with two $[Mn(tpaa)]^-$ anions that balance the charge (Figures 3 and S1). The $tpaa^{3-}$ ligands are triply deprotonated in all cases, as evidenced by C-O distances in the range 1.239(4) Å – 1.270(4) Å (Tables S7 and S8). Each Mn^{2+} ion in the structure can be considered as seven-coordinated, bonded to three pyridine N atoms, three carboxylate O atoms and the tertiary amine N atom of a $tpaa^{3-}$ ligand in a distorted capped octahedral geometry. Indeed, despite the long Mn–N_{tert} distance(s) (2.612 - 2.627 Å range), the presence of the Mn–N_{tert} bond is strongly supported by theoretical calculations (see below).

The geometry about the Mn^{2+} ion in the $[Mn(tpaa)]^-$ anion is similar to that found in $[\{Mn(tpaa)\}_2\{Ca(OH_2)_5(\mu\text{-}OH_2)\}_2]^{2+}$; however, Mn-N bonds in the latter are slightly longer than those in the former, the opposite being true for the Mn-O bond lengths for the two non-bridging carboxylates (Table 2). The presence of a Ca^{2+} ion coordinated via the bridging $\mu_{1,3}$ carboxylate moiety to the Mn^{2+} ion induces thus only a slight structural changes in the Mn coordination sphere. The Ca^{2+} ions are bonded by eight oxygen atoms of five terminal and

two bridging aqua ligands, and by a single carboxylate group in a distorted square antiprismatic geometry. The Ca-O distances lie in the range 2.427(2) Å – 2.530(2) Å, with one involving the bridging aqua ligands being the longest, and that of the carboxylate O atom the shortest. The geometry about each Ca^{2+} ion is distorted square antiprismatic and the Ca····Ca distance is 4.0335 Å. The two Mn····Ca distances within the cation are 5.807 Å and 6.113 Å, while the analogous distances between cation and anion are 6.623 Å and 8.556 Å. The Ca-bound aqua ligands are involved in significant H-bonding with the O atoms of the $tpaa^{3-}$ carboxylate groups within the cation and with the anion (Figure 3(b)), with O····O distances in the range 2.728(3) Å – 3.107(4) Å (Table S9). The generated H-bond network probably contributes in stabilizing the tetranuclear **Mn_2Ca_2** unit. The **Mn_2Ca_2·2Mn** structure underlines the stronger affinity of the $tpaa^{3-}$ ligand for a transition metal ion like Mn^{2+}, rather than for a closed-shell ion like Ca^{2+}. However, in the heteronuclear $[\{Mn(tpaa)\}_2\{Ca(OH_2)_5(\mu\text{-}OH_2)\}_2]^{2+}$ cation, each Ca^{2+} ions remains coordinated to one $tpaa^{3-}$ ligand through one bridging $\mu_{1,3}$-carboxylate.

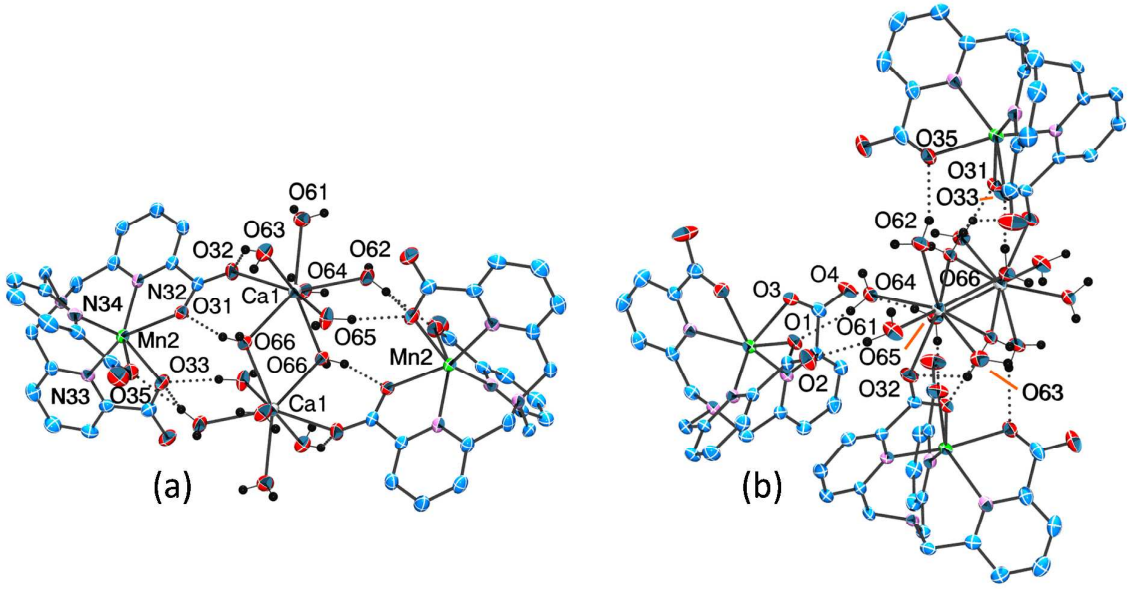

Figure 3. ORTEP drawings with thermal ellipsoids at 50% probability of the **Mn_2Ca_2·2Mn**·25H_2O complex; view of (a) the tetranuclear **Mn_2Ca_2** unit and the corresponding hydrogen bond network, and of (b) the **Mn_2Ca_2** unit associated to one **Mn** anion via H-bonds. Only relevant hydrogens are shown for clarity.

Table 2. Selected bond distances (Å) and angles (deg) for the **Mn_2Ca_2·2Mn**·25H_2O (**Mn_2Ca_2** cation and **Mn** anion) and **MnCa**·1.67MeOH·0.84H_2O complexes.

Mn_2Ca_2		**Mn**		**MnCa**·1.67MeOH·0.84H_2O	
Mn(2)-N(32)$_{pyr}$	2.297(3)	Mn(1)-N(2)$_{pyr}$	2.251(3)	Mn(1)-N(2)$_{pyr}$	2.226(2)
Mn(2)-N(33)$_{pyr}$	2.307(3)	Mn(1)-N(3)$_{pyr}$	2.262 (3)	Mn(1)-N(3)$_{pyr}$	2.245(2)
Mn(2)-N(34)$_{pyr}$	2.323(3)	Mn(1)-N(4)$_{pyr}$	2.287(3)	Mn(1)-N(4)$_{pyr}$	2.269(2)
Mn(2)-N(31)$_{tert}$	2.627(4)	Mn(1)-N(1)$_{tert}$	2.611(4)	Mn(1)-N(1)$_{tert}$	2.466(2)
Mn(2)-O(31)$_{\mu COO-}$	2.257(2)	Mn(1)-O(1)$_{COO-}$	2.233(2)	Mn(1)-O(1)$_{\mu COO-}$	2.2646(19)
Mn(2)-O(33)$_{COO-}$	2.226(2)	Mn(1)-O(3)$_{COO-}$	2.260(2)	Mn(1)-O(3)$_{\mu COO-}$	2.280(2)
Mn(2)-O(35)$_{COO-}$	2.230(2)	Mn(1)-O(5)$_{COO-}$	2.251(2)	Mn(1)-Cl(1)	2.5256(8)
Ca(1)-O(32)$_{\mu COO-}$	2.428(3)			Ca(1)-O(1)$_{\mu COO-}$	2.465(2)
Ca(1)-O(61)$_{OH2}$	2.472(3)			Ca(1)-O(3)$_{\mu COO-}$	2.4810(19)
Ca(1)-O(62)$_{OH2}$	2.470(3)			Ca(1)-O(21)$_{MeOH}$	2.410(2)
Ca(1)-O(63)$_{OH2}$	2.476(3)			Ca(1)-O(22)$_{MeOH}$	2.364(2)
Ca(1)-O(64)$_{OH2}$	2.427(2)			Ca(1)-O(23)$_{OH2}$	2.337(3)
Ca(1)-O(65)$_{OH2}$	2.487(3)			Ca(1)-O(25)$_{OH2}$	2.381(2)
Ca(1)-O(66)$_{\mu OH2}$	2.482(2)			Ca(1)-O(26)$_{OH2}$	2.355(2)
Ca(1)-O(66#)$_{\mu OH2}$	2.530(2)				
Ca(1)-Ca(1)#	4.0335(13)				

Complex [Mn(tpada)ClCa(H_2O)$_3$($MeOH$)$_2$]Cl·1.67MeOH·0.84H_2O (MnCa·1.67MeOH·0.84H_2O). The heteronuclear **MnCa** complex was formed by addition of of $MnCl_2$ (1.1 equivalents versus the initial amount of tpada ligand) in a methanolic solution of the dimeric **Ca_2** complex (Scheme 3(c,d)). In order to maintain the aqua ligands in the coordination sphere of Ca, a few drops of water were added. Single crystals of this compound were grown by slow diffusion of diisopropylether into this solution. As for **Mn_2Ca_2**, the complex is cationic. So, in both cases, charge balance is not the exclusive driving force for Ca binding to the Mn complex. The structure of **MnCa** consists of dinuclear unit in which the Mn^{2+} and Ca^{2+} ions are bridged by both carboxylate O atoms of the $tpada^{2-}$ ligand in a $\mu_{1,1}$ fashion (Figure 4). The cationic charge of the dinuclear is balanced by a chloride counterion. The four C-O distances in the range 1.239(4) Å – 1.279(3) Å support that the $tpada^{2-}$ ligand is fully deprotonated (Table S10). The Mn^{2+} ion is coordinated to the seven donor atoms of a tpada ligand to give an approximately pentagonal bipyramidal geometry around the metal ion; five donor atoms from the tpada ligand are close to coplanar with the Mn^{2+} ion, while the axial positions are occupied by the N atom of the unique pyridine moiety and by a chloride ion. As found in **Mn_2Ca_2·2Mn**, the Mn-N_{tert} bond is significantly longer (2.466(2) Å, versus

2.226(2) – 2.280(2) Å) than the other Mn-N and Mn-O bonds (Tables 2, S10), while the Mn-Cl distance (2.5256(8) Å) lies in the upper quartile of distances between a Mn^{2+} ion and a terminal Cl^- ligand. [52-54] The Ca^{2+} ion is coordinated by seven O atoms; two carboxylate from the tpada ligand, three aqua and two MeOH molecules. The X-ray structure also suggests slight H_2O/MeOH disorder in one of these coordination sites. The geometry around the Ca^{2+} ion is best described as distorted pentagonal bipyramidal, where one of the equatorial atoms (O(25)) lies somewhat below the pentagonal plane. Ca-O bond lengths range from 2.337(3) Å to 2.4810(19) Å, with those to the carboxylate O atoms being the longest ones. The Mn····Ca distance (3.8190(2) Å) is longer than that found in the other crystallographically characterized example of Mn-Ca in which an Mn^{2+} and a Ca^{2+} ion are bridged by two O atoms.[22, 27, 28] In contrast to the previous structures, **MnCa** displays only a limited H-bond network, with only the coplanar aquo ligand bridging with the two carboxylate of the ligand. Additional intramolecular H-bond with the chloride counterion as well as with MeOH and H_2O co-crystallized solvent ensure the overall stability.

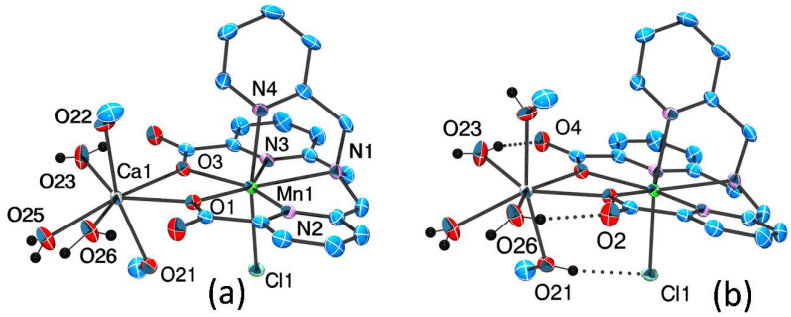

Figure 4. ORTEP drawing with thermal ellipsoids at 50% probability of **MnCa**·1.67MeOH·0.84H_2O; view of (a) the **MnCa** cation and (b) of the intramolecular hydrogen bond network. Only relevant hydrogens are shown for clarity

Also in this case, the Ca^{2+} ion, which was coordinated by five donor atoms of the tpada ligand in **Ca_2**, is displaced by the Mn^{2+} ion in the tripodal ligand. However, as for **Mn_2Ca_2**, the Ca^{2+} remains coordinated to the ancillary ligand through bridging carboxylate moieties. In addition, the Ca^{2+} ion in **MnCa** remains more strongly linked to the Mn^{2+} ion than in **Mn_2Ca_2** since in this case two $\mu_{1,1}$-bridging carboxylate couple the two cations instead of only one $\mu_{1,3}$-bridging carboxylate in **Mn_2Ca_2**. Consistently with a stronger Ca^{2+}-μ-COO^- interaction in **MnCa**, the Mn(1)-$O(1)_{\mu COO-}$ and Mn(1)-$O(3)_{\mu COO-}$ in **MnCa** (2.2646(2) and 2.280(2) Å, respectively) are slightly longer than Mn(2)-$O(31)_{\mu COO-}$ in **Mn_2Ca_2** (2.257(2) Å). A consequence of the stronger character of this carboxylate-mediated Mn-Ca interaction is that

the presence of Ca^{2+} has an effect of on the electronic properties of Mn^{2+}, as attested by EPR experiments (see below).

Theoretical calculations to analyze the nature of the N_{tert}-Mn bonding

The peculiar environment of the Mn^{2+} ion in the **MnCa** and **Mn_2Ca_2·2Mn** compounds, specifically the unusually long distance between the Mn ion and the N_{tert} atom of the tpada and tpaa ligands (2.47 Å and 2.63 Å, respectively), raises the question whether these species should be considered as genuine examples of seven-coordinate Mn complexes or not. To address this question we have performed quantum chemical calculations in order to analyze the nature of the bonding and the topology of the electron density of the two complexes.

A first approach to the problem is based on Mayer bond orders (MBOs),[55 56] which derive from a population analysis of the wave function. MBOs can be close to empirical bond orders expected for simple main group compounds, but they typically deviate strongly from integer values in transition metal complexes, where they serve instead as indicators of the distribution of bonding interactions around the central ion. In the present case, DFT calculations are consistent with the attribution of Mn–N_{tert} bonds, with computed MBOs of 0.32 and 0.38, respectively. These values are suggestive of weaker interactions compared with the average Mn–N_{py} bond orders of 0.64 and 0.56 in the two complexes, but they are similar to the MBOs for the Mn–O bonds, 0.34 and 0.36 for the tpada and 0.34–0.50 for the tpaa complex.

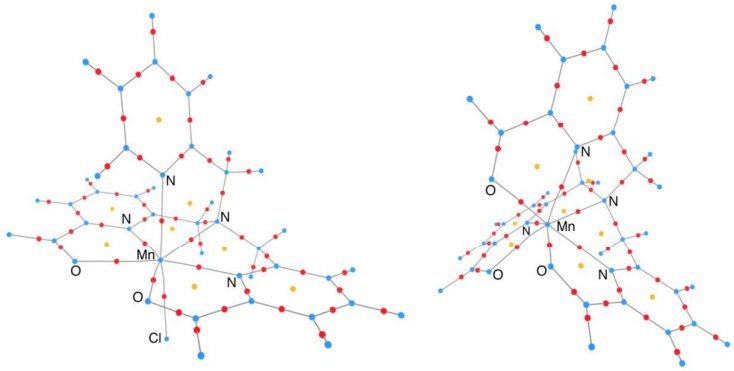

Figure 5. Partial molecular graphs derived from the topological analysis of the electron density for the **MnCa** (left) and the **Mn_2Ca_2** (right) complexes. Nuclear critical points are shown in blue, bond critical points in red, and ring critical points in yellow. Bond paths connecting the nuclear and bond critical points are plotted in grey.

Mayer bond orders are somewhat sensitive to the choice of basis set, so it is useful to examine an alternative definition that is based on the concept of "fuzzy" atoms, i.e. on partitioning the three-dimensional physical space into atomic regions without sharp boundaries.[57] Fuzzy bond orders (FBOs) are computed here using Becke's integration scheme.[58] For the tpada complex,

computed FBOs are 0.63 for Mn–N_{tert} versus ca. 0.93 on average for Mn–N_{py}, while for the tpaa complex the corresponding values are 0.51 and 0.88, respectively (average Mn–O FBOs are 0.83 and 0.93 for the two complexes). Despite the expected numerical differences of these distinct approaches, both agree on the relative magnitude of bond indices, with Mn–N_{tert} bonds being of lower order than Mn–N_{py}, but far from negligible. Therefore, despite the long Mn–N_{tert} distances, computed bond orders support the presence of Mn–N_{tert} bonds.

A complementary perspective is offered by the topological analysis of the electron density along the lines of the quantum theory of atoms in molecules (QTAIM).[59] This analysis locates critical points in the electron density, *i.e.* points where the gradient norm of the density is zero. Critical points are classified according to the number of negative eigenvalues of the Hessian matrix; of most importance are local maxima with three negative eigenvalues that are identified as nuclear critical points (NCPs), and saddle points with two negative eigenvalues called bond critical points (BCPs) because they generally arise between attractive atom pairs. The maximum gradient path that links a BCP with the two associated NCPs is defined as a "bond path" and is usually considered representative of a bonding interaction between the corresponding nuclei. The collection of all bond paths constitutes the so-called molecular graph of a molecule. Figure 5 depicts the computed molecular graphs for the two complexes under study (see also Figure S3 for a contour plot of the electron density within the N_3O_2 plane of the pentagonal bipyramidal Mn ion in the tpada complex). This analysis locates a BCP between Mn and N_{tert} in the computed electron density of both complexes, and shows clearly the presence of seven bond paths involving Mn. Finally, we note that the Laplacian of the electron density is negative at all Mn–N BCPs, suggesting that the nature of the interaction is the same, i.e. covalent for both Mn–N_{py} and Mn–N_{tert}.

Electronic properties of the manganese-calcium complexes by EPR spectroscopy

The electronic properties of the heteronuclear **Mn_2Ca_2·2Mn** and **MnCa** complexes involving seven-coordinate N_4O_3 and N_4O_2Cl Mn(II) ions, respectively, have been investigated by EPR spectroscopy as well as by density functional theory (DFT). The *D*-magnitudes for seven-coordinate Mn(II) ions are expected to be below 0.137 cm^{-1} (see Table 3).[60-62] Consequently, powder X and Q-band EPR spectra of these complexes have been recorded over a temperature range between 5 K and 298 K (Figures 6-8). While at X-band frequency, the EPR spectra are difficult to analyze, at Q-band frequency, the analysis became simpler due to the fact that the

high field limit condition is reached (*i.e.* the magnitude of D is much smaller than the energy of the microwave quantum provided by the spectrometer, $h\nu$ = 1.2 cm^{-1} / Q-band). The ZFS parameters can thus be estimated directly from the Q-band EPR spectra since the pattern of the spectra is only dependent on the ZFS and not on the anisotropy of the Zeeman interaction, which is very small for the Mn^{2+} ion (g-values close to 2.00).[60, 63, 64]

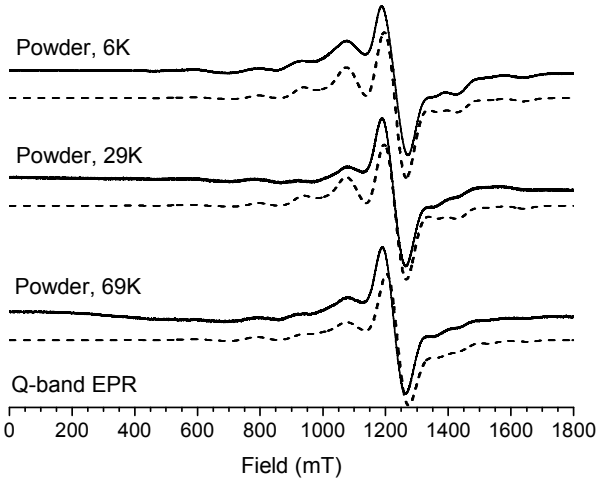

Figure 6. Experimental (solid line) and simulated (dashed line) Q-band EPR spectra recorded at different temperatures on powder of **MnCa**.

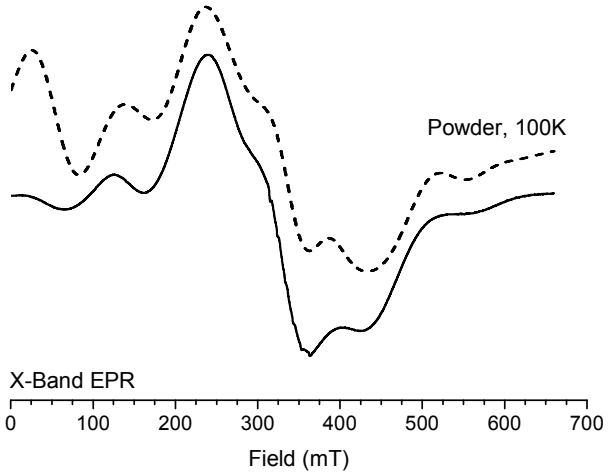

Figure 7. Experimental (solid line) and simulated (dashed line) X-band EPR spectra recorded at 100 K on powder of **MnCa**.

The powder Q-band EPR spectra of both Mn-Ca complexes can unambiguously be attributed to magnetically isolated Mn^{2+} ions at all temperatures, in accordance with the absence of magnetic coupling between the Mn^{2+} ions in these complexes.

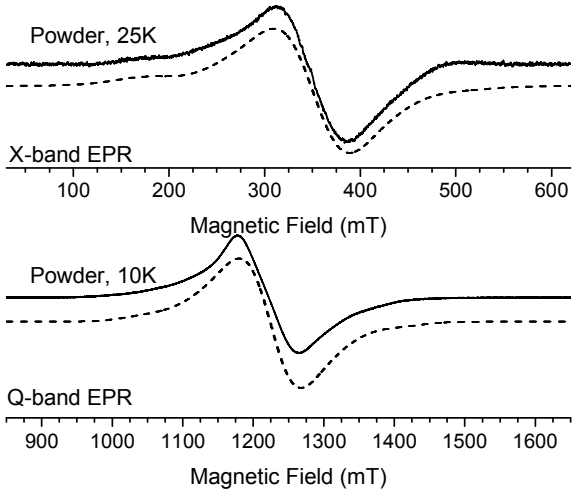

Figure 8. Experimental (solid line) and simulated (dashed line) X- and Q-band EPR spectra recorded on powder of **Mn_2Ca_2·2Mn**.

As expected for powder EPR spectra,[60, 63, 64] the ^{55}Mn hyperfine interactions are not resolved presumably because of intermolecular dipole-dipole interactions together with *D*-strain that contribute to the broadening of the line. As a consequence, the spin Hamiltonian parameters can be determined by simulating the experimental EPR spectra using a full-matrix diagonalization procedure of the simplified Hamiltonian displayed in Eq(1).

$$H = \mu_B \hat{\mathrm{B}} \cdot [g] \cdot \hat{S} + D(\hat{S}_z^2 - 1/3\hat{S}^2) + E(\hat{S}_x^2 - \hat{S}_y^2) \qquad (1)$$

While the first term represents the electronic Zeeman interaction, the last two define the second-order (bilinear) ZFS interaction with *D* and *E*, the axial and rhombic parts, respectively. In Table 3, the *D* and *E/D* parameters determined from the X- and Q-band EPR spectra of both compounds are summarized, together with those previously reported for seven-coordinate mononuclear Mn(II) complexes.

In the case of **MnCa**, the simulated EPR spectra nicely reproduce the experimental data, especially in the case of the Q-band spectra (Figure 6). On the other hand, as the high field limit condition is not reached at X-band frequency, transitions occur between mixed Zeeman

levels, leading to difficulty in precisely calculating their relative intensity (Figure 7). The sign of *D* has been unambiguously established from its low-temperature Q-band EPR spectra.

Table 3. Experimental ZFS parameters (*D* in cm^{-1} and *E/D*) of seven-coordinate Mn^{II} complexes.

Complex	coord. number	coord. sphere	D_{exp}[a]	E/D_{exp}	*ref*
MnCa (powder)	**7**	**N_4O_2Cl**	**-0.098**	**0.133**	this work
Mn_2Ca_2·2Mn (powder)	**7**	**N_4O_3**	**0.045**	**0.200**	this work
$[Mn(L^2_6)(OH_2)]$[b]	7	N_6O	-0.127	0	65
$[Mn(L)(OH_2)](ClO_4)_2$[c]	7	N_5O_2	0.137	0.093	62
$[Mn(terpy)(NO_3)_2(OH_2)]$[d]	7	N_3O_4	-0.068	0.147	61, 66
$[Mn(bpea)(NO_3)_2]$[e]	7	N_3O_4	+0.086	0.093	61, 66

[a]When determined, the sign of *D* is reported. [b] (L^2_6 = N,N,N′,N′ -tetra(2 pyridylmethyl)ethane-1,2-diamine. [c] L = N,N,N'-tris(2-methylpyridyl)-N'-hydroxyethyl-ethylenediamine. [d] terpy = 2,2';6',2''-terpyridine. [e] bpea = *N,N*-bis(2-pyridylmethyl)ethylamine.

In the case of **Mn_2Ca_2·2Mn**, the X- and Q-band EPR spectra are drastically less resolved than those of **MnCa** and display only one main feature centered at $g = 2.00$ (Figure 8). This can be rationalized by two complementary reasons. First, the spectra of **Mn_2Ca_2·2Mn** cover a small field range consistent with a small *D*-magnitude. Second, the EPR spectra of **Mn_2Ca_2·2Mn** result in the addition of the features associated with two types of Mn^{2+} ions, *i.e.* in the $[\{Mn(tpaa)\}_2\{Ca(OH_2)_4(\mu\text{-}OH_2)\}_2]^{2+}$ cation and in the $[Mn(tpaa)]^-$ anion, which display close geometries as revealed by the X-ray structure. The small structural modifications between the two types of Mn(II) can lead to minor changes in the ZFS parameters, and thus to a broadening of the lines. However, while the ZFS parameters cannot be distinguished between the two types of Mn(II) ions, the EPR spectra are not totally uninformative and the ZFS can be estimated (Table 3), but not the sign of *D*. Unlike for Jahn-Teller ion such as Mn(III), the *D*-sign is not correlated to structural properties for Mn(II) complexes.[60]

The *D*-magnitude of 0.098 cm^{-1} and 0.045 cm^{-1} found for the Mn^{2+} ions in **MnCa** and **Mn_2Ca_2·2Mn,** respectively, fall in the range of the *D*-values reported previously for seven-coordinate mononuclear Mn(II) complexes (Table 3). The number of such complexes is however limited to a few examples with a N/O coordination sphere and, as for six-coordinate Mn(II) complexes with similar coordination sphere, no trend between *D* magnitude and N/O ratio can be found.[61, 67] The larger *D*-value found for **MnCa** compared to **Mn_2Ca_2·2Mn** can be attributed to several factors including the presence of a chloride anion in the coordination

sphere of the Mn(II) ion, the different N/O ratio and the effect of Ca^{2+} strongly bounded to the Mn^{2+} ion *via* two $\mu_{1,1}$-carboxylato bridges. It has been previously shown that halide anions lead to an increase of *D* in the case of five- and six-coordinate Mn(II) ions,[54, 65] but no such correlation is available for seven-coordinate compounds.

To further investigate the electronic properties of these complexes, DFT calculations have been performed with the aim of predicting the ZFS and investigating the potential effect of the Ca^{2+} ion on the ZFS of the Mn^{2+} ion. These calculations have been carried out on optimized structures in which only the positions of the hydrogen atoms were relaxed. It has been shown *via* systematic investigation that the ZFS of Mn^{2+} ions with various types of coordination spheres (for five and six-coordinate Mn^{2+} ions with various types of ligands such as halides, N-, O- and /or S-based donor atoms) can be reasonably predicted by DFT calculations.[67-69] In the case of seven-coordinate complexes, *D* has been predicted for only three other complexes with varying degrees of success (Table 3 and experimental section). Consequently, only the comparison of *D* calculated in each series (tpaa and tpada) can be discussed.

Concerning **MnCa**, calculations have been performed on optimized structures initiated from the **MnCa** complex (without the counter anion), and also from its {Mn(tpada)Cl} part. In the case of **Mn_2Ca_2·2Mn**, structures have been optimized from the experimental data of the $[Mn(tpaa)]^-$ anion as well as the $\{Mn(tpaa)Ca(OH_2)_7\}$ and {Mn(tpaa)} parts of the $[\{Mn(tpaa)\}_2\{Ca(OH_2)_5(\mu\text{-}OH_2)\}_2]^{2+}$ unit. All corresponding calculated ZFS parameters are reported in Table 4 together with the two different contributions to *D*, *i.e.* the spin-spin interaction (D_{SS}) and spin orbit coupling (D_{SOC}). As previously observed,[54, 61, 70] the D_{SOC} represents the major contribution to *D*, but in the case of small *D*-values, the D_{SS} contribution is not negligible (up to about 25%). Looking at the *D*-values calculated for the Mn tpaa structures, it can be noticed that they are very close to each other, especially when comparing the $[Mn(tpaa)]^-$ ion and the $\{Mn(tpaa)Ca(OH_2)_7\}$ part. This is in agreement with the fact that the two types of Mn^{2+} ion in **Mn_2Ca_2·2Mn** cannot be distinguished based on the EPR data. Besides, the *D*-values calculated on the {Mn(tpaa)} and $\{Mn(tpaa)Ca(OH_2)_7\}$ moieties issued from the $[\{Mn(tpaa)\}_2\{Ca(OH_2)_5(\mu\text{-}OH_2)\}_2]^{2+}$ unit are also very close suggesting that the Ca^{2+} ion has no significant effect on the electronic properties of the Mn^{2+} ion, when linked to a $\mu_{1,3}$-carboxylato bridged.

For **MnCa**, there is a good agreement between the experimental and calculated *D*-magnitude (-0.98 *versus* +0.107 cm^{-1}) (Tables 3 and 4) even if the sign is inverse because of its large *E/D*

ratio (predictions are unreliable for $E/D>0.2$).[69] Interestingly, the D-magnitude calculated on the {Mn(tpada)Cl} moiety (D_{calc} = +0.143 cm^{-1}) is notably larger than that calculated on the $[Mn(tpada)ClCa(H_2O)_3(MeOH)_2]^+$ complex, suggesting that the Ca^{2+} ion have an effect on the ZFS parameters of the neighboring Mn(II) ion. This apparent contrasting result with respect to what was observed with **Mn_2Ca_2·2Mn**, could be rationalized by the fact that, in **MnCa**, the Ca^{2+} ion is much more strongly bound to the Mn^{2+} ion, *i.e. via* two $\mu_{1,1}$-carboxylato bridges *versus* one $\mu_{1,3}$-carboxylato bridge in **Mn_2Ca_2·2Mn** leading to a shorter Mn···Ca distance in **MnCa** than in **Mn_2Ca_2·2Mn** (3.8190(2) Å and 6.1129(10) Å, respectively).

Table 4. DFT calculated ZFS values for different optimized structures, in which only the hydrogen atoms were relaxed, related to **Mn_2Ca_2·2Mn** and **MnCa**.

Optimized structures	D_{calc}	D_{SS}	D_{SOC}	E_{calc}	E/D_{calc}
tpaa					
{Mn(tpaa)Ca$(OH_2)_7$} part	-0.090	-0.020	-0.070	-0.012	0.026
{Mn(tpaa)} part in **Mn_2Ca_2**	-0.094	-0.020	-0.074	-0.012	0.123
$[Mn(tpaa)]^-$	-0.089	-0.020	-0.069	-0.002	0.025
tpada					
MnCa	+0.107	+0.009	+0.098	+0.028	0.261
{Mn(tpada)Cl} part	+0.143	+0.010	+0.133	+0.017	0.119

Both complexes have been dissolved in MeOH and X-band EPR spectra have been recorded on the corresponding solutions (Figures S4 and S5). As it can be seen, only the spectra for the **MnCa** are notably different than those recorded on the respective powder, evidencing that some structural modifications occur for this complex that can be due to the release in solution of Ca^{2+} and/or of Cl^-. For **Mn_2Ca_2·2Mn**, the similarity of the spectra in solid state and in solution does not allow to conclude on a real dissociation of calcium, the latter having no significant effect on the electronic parameters of the linked Mn(II) (μ1,3-carboxylate bridge).

Concluding remarks

In this work, we have isolated, structurally characterized and studied the EPR properties of heterometallic manganese(II)-calcium(II) complexes with two carboxylate-functionalized tripodal tris(2-pyridylmethyl)amine ligands: the previously reported heptadentate H_3tpaa and the new hexadentate H_2tpada. Carboxylate functions incorporated in the periphery of the ligands framework facilitate the binding of calcium to the manganese units to generate rare examples of carboxylate-bridged Mn(II)-Ca(II) complexes, **Mn_2Ca_2·2Mn** and **MnCa**. These complexes may be relevant for mimicking the first stages of the OEC assembly process. Since

these heterometallic complexes are both cationic species, the charge balance cannot be considered as the exclusive driving force for Ca binding to the Mn units. Interestingly, the presence of two or three carboxylate groups in the supporting ligands influences the calcium binding mode to the manganese-containing fragment: two $\mu_{1,1}$-bridging carboxylates couple the Mn(II) and Ca^{2+} in **MnCa**, while only one $\mu_{1,3}$-carboxylate bridge connects each Ca^{2+} ion to each Mn(II) in $\mathbf{Mn_2Ca_2}$. As a result, the Ca^{2+} ion is more strongly linked to the Mn^{2+} ion in **MnCa** than in $\mathbf{Mn_2Ca_2}$ and can thus have an effect its electronic structure. Indeed, solid state EPR spectroscopy, combined with DFT calculations, clearly shows that the Ca^{2+} ion influences the ZFS parameters of the $\mu_{1,1}$-carboxylates bridged Mn(II) ion in **MnCa**. Remarkably, the **MnCa** complex represents a rare example of complex containing a $\mu_{1,1}$-carboxylate bridge between Mn and Ca ions[39] and of a small nuclearity binuclear Mn-Ca complex.[32]

In this work, we also succeed to structurally characterize the corresponding homometallic calcium(II) complexes, $\mathbf{Ca_1}$ and $\mathbf{Ca_2}$, As expected, by comparing these species and the heterometallic Mn-Ca species, it is evident that Mn^{2+} ion, when present in solution, easily replaces calcium in the first coordination sphere of the supporting ligand.

All the reported X-ray structures corroborate the high tendency of calcium to coordinate water molecules. Actually, a variable number (n = 1-7) of water molecules are coordinated to Ca in the $\mathbf{Ca_1}$, $\mathbf{Ca_2}$, $\mathbf{Mn_2Ca_2}$**·2Mn** and **MnCa** complexes. For comparison, the PSII structure shows the presence of two water molecules coordinated to calcium.[71] In analogy to what is observed in the OEC, most of the Ca-bound aquo ligands in our complexes are involved in hydrogen-bond networks. The presence of these H-bonds could significantly contribute to stabilize the binding of water molecules on Ca^{2+}.

Finally, in all of these complexes, the H_3tpaa and H_2tpada ligands act as heptadentate and hexadentate ligands, respectively, towards Mn(II) and Ca(II). Actually, the coordination of the central tertiary amine nitrogen atom to these metal ions, although unusually long due to the constraint geometry of the ligands, has been attested by X-ray diffraction data and confirmed by theoretical calculations in the case of Mn^{2+}. As a consequence, the manganese coordination sphere is saturated in the presence of the H_3tpaa ligand, while the lower denticity of H_2tpada offers a labile coordination site to Mn, which is occupied by a chloride anion in the case of **MnCa**. With this respect, the possibility to employ **MnCa** as precursor for generating high-valent heterometallic Ca-$Mn^{III/IV}$-oxo complexes, more relevant to the OEC, with the oxo ligands occupying the labile sites of Mn, is currently under investigation in our laboratory.

Experimental details

The [Ca(Htpaa)(OH_2)] (**Ca_1**) and [{Mn(tpaa)}$_2${Ca(OH_2)$_5$(μ-OH_2)}$_2$][Mn(tpaa)]$_2$ (**Mn_2Ca_2·2Mn**) complexes were prepared according to a reported procedure.[46] 2-bromomethyl-6-pyridine carboxylic acid methyl ester was prepared from dimethyl 2,6-pyridinedicarboxylate in a two-step reported procedure.[72] Acetonitrile was degassed prior to use. All other reagents and solvents were used as received. The synthesis of compound Me_2tpada was performed under argon (Schlenk techniques). The NMR spectra were recorded on a Bruker Avance III 400 MHz spectrometer using standard Bruker pulse sequences. The elemental analyses were carried out with a C, H, N analyzer (SCA, CNRS).

Synthesis of ligands and complexes

Synthesis of dimethyl 6,6'-(pyridin-2-ylmethylazanediyl)bis(methylene)dipicolinate (Me_2tpada). 2-Picolylamine (450 μL, 4.36 mmol) and anhydrous K_2CO_3 (2.40 g, 17.37 mmol) were successively added to a solution of 2-bromomethyl-6-pyridine carboxylic acid methyl ester (2.0 g, 8.69 mmol) in acetonitrile (50 mL). This mixture was heated to 60 ºC for 45 min. After cooling to 25 ºC, the excess of salts was filtered off over Celite and the residual orange solution was evaporated to dryness. The crude product was redissolved in ethyl acetate (200 mL) and washed with water (2 x 100 mL) and brine (100 mL). After drying the organic phase with $MgSO_4$ and evaporation of the solvent, the product was recrystallized from an ethyl acetate: cyclohexane mixture. The resulting white powder was filtered and collected. The filtrate was evaporated to dryness and the recrystallization process was repeated three times. The solids were combined, washed with cyclohexane (5 mL), dried and collected as a white powder, corresponding to Me_2tpada (yield, 1.14 g, 65%). ^{1}H NMR (400 MHz, $CDCl_3$): δ 8.54 (d, *J* = 4.5 Hz, 1H), 7.98 (d, *J* = 7.5 Hz, 2H), 7.86 (d, *J* = 7.5 Hz, 2H), 7.80 (t, *J* = 7.5 Hz, 2H), 7.64 (t, *J* = 7.6 Hz, 1H), 7.54 (d, *J* = 7.6 Hz, 1H), 7.15 (t, *J* = 5.7 Hz, 1H), 4.02 (s, 4H), 3.99 (s, 6H), 3.90 (s, 2H). ^{13}C NMR (100 MHz, $CDCl_3$): δ 166.0, 160.2, 159.0, 149.4, 147.6, 137.5, 136.6, 126.3, 123.8, 123.3, 122.3, 60.3, 60.1, 53.0.

Synthesis of 6,6'-(pyridin-2-ylmethylazanediyl)bis(methylene)dipicolinic acid (H_2tpada). A solution of LiOH (113 mg, 4.72 mmol) in water (5 mL) was added to a solution of Me_2tpada (481 mg, 1.18 mmol) in THF (5 mL) in a microwave vessel (35 mL). The mixture was heated to 130 ºC under microwave irradiation for 30 min. After cooling to 25 ºC, THF was removed under vacuum. HPF_6 (~ 55%, 1.2 mL) was slowly added to the resulting

aqueous solution under stirring. After addition of isopropanol (10 mL), the mixture was stirred for 15 h. A white precipitate was formed, it was filtered, washed with isopropanol and dried under vacuum, in presence of P_2O_5 (yield, 410 mg, 53%). Anal. Calcd. for $C_{20}H_{18}N_4O_4 \cdot 1.8HPF_6 \cdot H_2O$ (659.15): C, 36.44; H, 3.33; N, 8.50. Found: C, 36.71; H, 3.40; N, 8.59. ^{1}H NMR (400 MHz, CD_3OD): δ 9.01 (d, *J* = 5.4Hz, 1H), 8.25 (t, *J* = 7.7Hz, 1H), 8.02 (d, *J* = 7.7Hz, 2H), 7.90 (t, *J* = 7.8 Hz, 2H), 7.78-7.73 (m, 2H), 7.58 (d, *J* = 7.7 Hz, 2H), 4.49 (s, 2H), 4.35 (s, 4H). ^{13}C NMR (100 MHz, CD_3OD): δ167.0, 158.3, 148.9, 145.5, 144.9, 140.0, 128.4, 127.0, 126.2, 125.3, 60.6, 57.8. ^{31}P NMR (162 MHz, CD_3OD): δ -143.2 (sept, *J* = 707 Hz). ^{19}F NMR (376 MHz, CD_3OD): δ -73.3 (d, *J* = 707 Hz).

Synthesis of $[Ca(tpada)(OH_2)_2]_2$ (Ca_2). A saturated aqueous solution of $Ca(OH)_2$ was added to a suspension of $H_2tpada \cdot 1.8HPF_6 \cdot H_2O$ (32.0 mg, 48.54 μmol) in water (3 mL) until pH ~ 8 was reached. During the addition, the complete dissolution of the ligand was observed, followed by the formation of a white precipitate. After 10 min, methanol (5 mL) was added to the reaction mixture, resulting in the complete dissolution of the precipitate under stirring. After few days, X-Ray suitable colorless single crystals of $\mathbf{Ca_2} \cdot 5.2H_2O$ were obtained by slow evaporation of the solvent from this solution. These were filtered, washed with cold water (1 mL) and air-dried for few days (yield, 6.6 mg, 30%). Anal. Calcd. for $C_{40}H_{40}N_8O_{12}Ca_2 \cdot 0.75H_2O$ (918.46): C, 52.31; H, 4.55; N, 12.20. Found: C, 52.26; H, 4.40; N, 12.21.

Synthesis of $[Mn(tpada)ClCa(OH_2)_{2.67}(MeOH)_{2.33}]Cl$ (MnCa). A saturated aqueous solution of $Ca(OH)_2$ was added to a suspension of $H_2tpada \cdot 1.8HPF_6 \cdot H_2O$ (132.7 mg, 201.32 μmol) in water (20 mL) until pH ~8 was reached, yielding a white precipitate. This was filtered, air-dried and redissolved in methanol (20 mL). Solid $MnCl_2$ (27.6 mg, 219.32 μmol) was added. The resulting pale yellow solution was stirred for 30 minutes and a droplet of water was added. Clusters of pale yellow needle-shaped X-Ray suitable crystals of $\mathbf{MnCa} \cdot 1.67CH_3OH \cdot 0.84H_2O$ were obtained by slow diffusion of isopropyl ether on the latter solution over a week. These were filtered, washed with isopropyl ether (2 mL) and dried under vacuum (yield, 51.0 mg, 42%). Anal. Calcd. for $C_{20}H_{22}N_4O_7MnCaCl_2$ (596.33): C, 40.28; H, 3.72; N, 9.39. Found: C, 40.03; H, 3.75; N, 9.33.

X-ray structure determination

Single-crystal diffraction data were collected on an Oxford-Diffraction XCalibur S Kappa geometry diffractometer (MoKα radiation, graphite monochromator, λ 0.71073Å). The

CrysAlisPro program package (Agilent Technologies) was used for cell refinements and data reductions. For all complexes an absorption correction (CrysAlisPro) was applied to the data. The molecular structures were solved by charge flipping method (Superflip)[73] for **1**, **2** and **3**, by direct methods for **4** and refined on F2 by full matrix least-squares techniques using SHELXLTl in OLEX 2.1.65 software environment.[74] For all complexes, all non-hydrogen atoms were refined anisotropically. For **Ca_2**, all hydrogens were found by Fourier transformation and refined with individual isotropic displacement parameters. For **MnCa**, all hydrogens were placed at their calculated positions, except for the hydroxyl of methanol ligands containing O21, O22 and O31 and aquo ligands containing O23, O25 and O26, which were found. CCDC 995925 and CCDC 995924 contain the supplementary crystallographic data for **Ca_2**·5.2H_2O and **MnCa**·1.67CH_3OH·0.84H_2O, respectively. A summary of X-ray data collection and structure refinement for all complexes is reported in Tables S1 and S6. Selected bond distances and angles are provided in Tables S2, S4, S7, S8 and S10 and hydrogen bonds lengths and angles in Tables S3, S5, S9 and S11.

EPR spectroscopy

Powder X-band EPR spectra were recorded with a Bruker EMX, equipped with an ER-4192 ST Bruker cavity and an ER-4131 VT for the 100 K experiments. Powder Q-band EPR spectra were recorded with an ER-5106 QTW Bruker cavity and an Oxford Instruments ESR-900 continuous-flow helium cryostat for the Q-band for the 4.5 K experiments. The spectra have been simulated by using the easyspin program supported by Matlab.[75] All spectra have been simulated using the spin Hamiltonian Eq(1) even the X-band EPR spectrum of **MnCa** recorded in solution. Our aim being to determine the ZFS parameters, Eq(1) has been used to simulate the data, even if hyperfine lines of the Mn ion in several transitions are unresolved in such conditions. Indeed, the hyperfine coupling interaction related to the Mn ion is uninformative with respect to its structural and electronic properties.[67]

Computational details

All calculations were performed with ORCA,[76] using dense integration grids (Grid6 in ORCA convention) and tight SCF convergence criteria. The structural models used for the computational study of the bonding in the reported complexes were cleaned-up versions of the crystallographic models, where counterions and solvent molecules were removed, single orientations of disordered groups were selected, and only one Mn site and associated Ca ions

with complete hydration were considered. The complete models are shown in Figure S2. In order to probe the crystallographic configuration as closely as possible, only the hydrogen atoms were optimized. This strategy has been successfully adopted in other reported systems.[68, 69, 77, 78] The TPSS functional[79] was used in combination with def2-TZVP basis sets[80] and the corresponding auxiliary Coulomb fitting basis sets[81] in completely decontracted form. Topological analysis of the electron density was performed with the program MultiWFN[82] and the molecular graphs depicting critical points and paths were visualized with VMD.[83] Regarding the ZFS prediction, the ZFS parameters have been calculated on X-ray structures as well as from optimized structures in which only the positions of the hydrogen atoms were relaxed. For a discussion of this point see references.[69, 77, 78, 84] The ZFS calculations based on DFT were performed with the non-hybrid BP86[85, 86] functionals using the TZVP basis set[87] and taking advantage of the RI approximation with the auxiliary TZV/J Coulomb fitting basis sets.[81] It has been previously demonstrated that while the quality of the prediction is slightly better with the B3LYP functional for halide Mn^{II} complexes, for Mn^{II} complexes containing only N-and O-based ligands, BP86 is notably superior.[61, 69] Therefore, only data calculated using BP86 are reported in Table 4. In all cases, the prediction of *D* is notably overestimated. Such results have been previously observed when Mn(II) ions with small *D* are involved. This can be rationalized by the fact that the prediction of *D* is based on the calculations of different contributions that are of the same order of magnitude but have partially opposing signs and different physical contents. Consequently, the smaller the *D*-magnitude is, the more difficult its prediction.[54]

Acknowledgements

B.G. thanks the "Université Joseph Fourier of Grenoble" for his PhD grant. The Authors acknowledge for financial support the LABEX ARCANE (ANR-11-LABX-0003-01) for the project MnCaPSII, the french Agence Nationale de la Recherche (ANR-13-BS07-0015-01 (MnCaOEC) and ANR-09-JCJC-0087 (MANGACOM)). Acknowledgment to Reseau National de RPE interdisciplinaire TGE CNRS for EPR measurement facilities. This work was also supported by ICMG FR 2067 and COST CM1202 program (PERSPECT H_2O).

TOC

Rare examples of heteronuclear μ-carboxylato bridged Mn-Ca complexes were isolated from tripodal ligands that incorporate carboxylate functions.

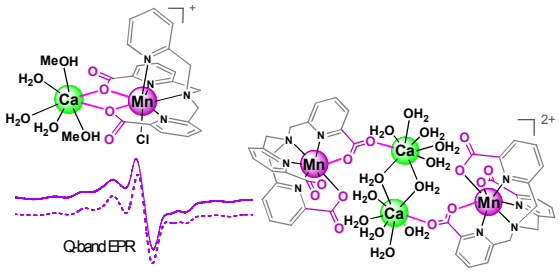

References

1. J. Yano and V. Yachandra, *Chem. Rev.*, 2014, **114**, 4175-4205.
2. N. Cox, D. A. Pantazis, F. Neese and W. Lubitz, *Acc. Chem. Res.*, 2013, **46**, 1588-1596.
3. D. J. Vinyard, G. M. Ananyev and G. C. Dismukes, *Annu. Rev. Biochem.*, 2013, **82**, 577-606.
4. M. Suga, F. Akita, K. Hirata, G. Ueno, H. Murakami, Y. Nakajima, T. Shimizu, K. Yamashita, M. Yamamoto, H. Ago and J.-R. Shen, *Nature*, 2015, **517**, 99-U265.
5. Y. Umena, K. Kawakami, J.-R. Shen and N. Kamiya, *Nature*, 2011, **473**, 55-U65.
6. T. Lohmiller, V. Krewald, M. P. Navarro, M. Retegan, L. Rapatskiy, M. M. Nowaczyk, A. Boussac, F. Neese, W. Lubitz, D. A. Pantazis and N. Cox, *Phys. Chem. Chem. Phys.*, 2014, **16**, 11877-11892.
7. H. Nilsson, F. Rappaport, A. Boussac and J. Messinger, *Nature Communications*, 2014, **5**.
8. P. E. M. Siegbahn, *Phys. Chem. Chem. Phys.*, 2014, **16**, 11893-11900.
9. L. Vogt, M. Z. Ertem, R. Pal, G. W. Brudvig and V. S. Batista, *Biochemistry*, 2015, **54**, 820-825.
10. V. Krewald, M. Retegan, N. Cox, J. Messinger, W. Lubitz, S. DeBeer, F. Neese and D. A. Pantazis, *Chem. Sci.*, 2015, **6**, 1676-1695.
11. R. Chatterjee, S. Milikisiyants, C. S. Coates, F. H. M. Koua, J.-R. Shen and K. V. Lakshmi, *Phys. Chem. Chem. Phys.*, 2014, **16**, 20834-20843.
12. X. Li and P. E. M. Siegbahn, *Phys. Chem. Chem. Phys.*, 2015, DOI: 10.1039/C5CP00138B, Ahead of Print.
13. N. Cox, M. Retegan, F. Neese, D. A. Pantazis, A. Boussac and W. Lubitz, *Science*, 2014, **345**, 804-808.
14. C. F. Yocum, *Coord. Chem. Rev.*, 2008, **252**, 296-305.
15. S. Mukhopadhyay, S. K. Mandal, S. Bhaduri and W. H. Armstrong, *Chem. Rev.*, 2004, **104**, 3981-4026.
16. C. S. Mullins and V. L. Pecoraro, *Coord. Chem. Rev.*, 2008, **252**, 416-443.
17. C. W. Cady, R. H. Crabtree and G. W. Brudvig, *Coord. Chem. Rev.*, 2008, **252**, 444-455.
18. M.-N. Collomb and A. Deronzier, *Eur. J. Inorg. Chem.*, 2009, 2025-2046.
19. M. Wiechen, H. M. Berends and P. Kurz, *Dalton Trans.*, 2012, **41**, 21-31.
20. M. Hirahara, A. Shoji and M. Yagi, *Eur. J. Inorg. Chem.*, 2014, **2014**, 595-606.
21. M. D. Karkas, O. Verho, E. V. Johnston and B. Akermark, *Chem. Rev.*, 2014, **114**, 11863-12001.
22. A. Mishra, W. Wernsdorfer, K. A. Abboud and G. Christou, *Chem. Commun.*, 2005, 54-56.
23. A. Mishra, J. Yano, Y. Pushkar, V. K. Yachandra, K. A. Abboud and G. Christou, *Chem. Commun.*, 2007, 1538-1540.
24. S. Mukherjee, J. A. Stull, J. Yano, T. C. Stamatatos, K. Pringouri, T. A. Stich, K. A. Abboud, R. D. Britt, V. K. Yachandra and G. Christou, *Proceedings of the National Academy of Sciences of the United States of America*, 2012, **109**, 2257-2262.
25. E. S. Koumousi, S. Mukherjee, C. M. Beavers, S. J. Teat, G. Christou and T. C. Stamatatos, *Chem. Commun.*, 2011, **47**, 11128-11130.
26. A. A. Alaimo, D. Takahashi, L. Cunha-Silva, G. Christou and T. C. Stamatatos, *Inorg. Chem.*, 2015, **54**, 2137-2151.
27. L. B. Jerzykiewicz, J. Utko, M. Duczmal and P. Sobota, *Dalton Trans.*, 2007, 825-826.
28. I. J. Hewitt, J. K. Tang, N. T. Madhu, R. Clérac, G. Buth, C. E. Anson and A. K. Powell, *Chem. Commun.*, 2006, 2650-2652.
29. H. Fliegl, K. Fink, W. Klopper, C. E. Anson, A. K. Powell and R. Clérac, *Phys. Chem. Chem. Phys.*, 2009, **11**, 3900-3909.
30. S. Nayak, H. P. Nayek, S. Dehnen, A. K. Powell and J. Reedijk, *Dalton Trans.*, 2011, **40**, 2699-2702.
31. C. Chen, C. Zhang, H. Dong and J. Zhao, *Dalton Trans.*, 2015, **44**, 4431-4435.
32. Y. J. Park, J. W. Ziller and A. S. Borovik, *J. Am. Chem. Soc.*, 2011, **133**, 9258-9261.
33. J. S. Kanady, E. Y. Tsui, M. W. Day and T. Agapie, *Journal*, 2011, **333**, 733-736.

34. E. Y. Tsui, J. S. Kanady and T. Agapie, *Inorg. Chem.*, 2013, **52**, 13833-13848.
35. E. Y. Tsui, R. Tran, J. Yano and T. Agapie, *Nature Chemistry*, 2013, **5**, 293-299.
36. J. S. Kanady, P.-H. Lin, K. M. Carsch, R. J. Nielsen, M. K. Takase, W. A. Goddard, III and T. Agapie, *J. Am. Chem. Soc.*, 2014, **136**, 14373-14376.
37. I. G. de Muro, M. Insausti, L. Lezama, M. K. Urtiaga, M. I. Arriortua and T. Rojo, *Journal of the Chemical Society-Dalton Transactions*, 2000, 3360-3364.
38. N. Li, M. Wang, C. B. Ma, M. Q. Hu, R. W. Zhou, H. Chen and C. N. Chen, *Inorg. Chem. Commun.*, 2010, **13**, 730-732.
39. V. Kotzabasaki, M. Siczek, T. Lis and C. J. Milios, *Inorg. Chem. Commun.*, 2011, **14**, 213-216.
40. A. C. Benniston, S. Melnic, C. Turta, A. B. Arauzo, J. Bartolome, E. Bartotome, R. W. Harrington and M. R. Probert, *Dalton Trans.*, 2014, **43**, 13349-13357.
41. C. Zhang, C. Chen, H. Dong, J.-R. Shen, H. Dau and J. Zhao, *Science*, 2015, **348**, 690-693.
42. J. Dasgupta, G. M. Ananyev and G. C. Dismukes, *Coord. Chem. Rev.*, 2008, **252**, 347-360.
43. M. M. Najafpour, M. Fekete, D. J. Sedigh, E.-M. Aro, R. Carpentier, J. J. Eaton-Rye, H. Nishihara, J.-R. Shen, S. I. Allakhverdiev and L. Spiccia, *ACS Catal.*, 2015, **5**, 1499-1512.
44. J. E. Bartlett, S. V. Baranov, G. M. Ananyev and G. C. Dismukes, *Philos. Trans. R. Soc., B*, 2008, **363**, 1253-1261.
45. Y. Bretonniere, M. Mazzanti, J. Pecaut, F. A. Dunand and A. E. Merbach, *Chem. Commun.*, 2001, 621-622.
46. V. Martin-Diaconescu, M. Gennari, B. Gerey, E. Tsui, J. Kanady, R. Tran, J. Pecaut, D. Maganas, V. Krewald, E. Goure, C. Duboc, J. Yano, T. Agapie, M.-N. Collomb and S. DeBeer, *Inorg. Chem.*, 2015, **54**, 1283-1292.
47. Y. Bretonniere, M. Mazzanti, J. Pecaut, F. A. Dunand and A. E. Merbach, *Inorg. Chem.*, 2001, **40**, 6737-6745.
48. A. Pellissier, Y. Bretonniere, N. Chatterton, J. Pecaut, P. Delangle and M. Mazzanti, *Inorg. Chem.*, 2007, **46**, 3714-3725.
49. E. L. Muetterties and L. J. Guggenberger, *J. Am. Chem. Soc.*, 1974, **96**, 1748-1756.
50. E. C. Constable, *Progress in Inorganic Chemistry, Vol 42*, 1994, **42**, 67-138.
51. A. G. Blackman, *Comptes Rendus Chimie*, 2005, **8**, 107-119.
52. *Cambridge Structural Database, Version 5.35, CCDC, UK.*, 2014.
53. I. Romero, M.-N. Collomb, A. Deronzier, A. Llobet, E. Perret, J. Pécaut, L. L. Pape and J.-M. Latour, *Eur. J. Inorg. Chem.*, 2001, 69-72.
54. C. Duboc, T. Phoeung, S. Zein, J. Pecaut, M. N. Collomb and F. Neese, *Inorg. Chem.*, 2007, **46**, 4905-4916.
55. I. Mayer, *Int. J. Quantum Chem*, 1984, **26**, 151-154.
56. A. J. Bridgeman, G. Cavigliasso, L. R. Ireland and J. Rothery, *J. Chem. Soc., Dalton Trans.*, 2001, 2095-2108.
57. I. Mayer and P. Salvador, *Chem. Phys. Lett.*, 2004, **383**, 368-375.
58. A. D. Becke, *J. Chem. Phys.*, 1988, **88**, 2547-2553.
59. R. F. W. Bader, in *Atoms in Molecules: A Quantum Theory*, Oxford University Press: Oxford, 1990, p. 458.
60. C. Duboc, M. N. Collomb and F. Neese, *Appl. Magn. Reson.*, 2010, **37**, 229-245.
61. J. Rich, C. E. Castillo, I. Romero, M. Rodriguez, C. Duboc and M. N. Collomb, *Eur. J. Inorg. Chem.*, 2010, DOI: 10.1002/ejic.201000373, 3658-3665.
62. C. A. Wegermann, P. Strapasson, S. M. M. Romanowski, A. Bortoluzzi, R. R. Ribeiro, F. S. Nunes and S. M. Drechsel, *Applied Catalysis a-General*, 2013, **454**, 11-20.
63. J. R. Pilbrow, in *Transition Ion Paramagnetic Resonance*, Clarendon Press, Oxford, 1990.
64. F. E. Mabbs and D. Collison, in *Electron Paramagnetic Resonance of d Transition Metal Compounds, chapter 12*, Elsevier, Amsterdam, 1992.
65. C. Hureau, S. Groni, R. Guillot, G. Blondin, C. Duboc and E. Anxolabehere-Mallart, *Inorg. Chem.*, 2008, **47**, 9238-9247.
66. C. Baffert, I. Romero, J. Pecaut, A.Llobet, A. Deronzier and M.-N. Collomb, *Inorg. Chim. Acta*, 2004, **357**, 3430-3436.

67. C. Duboc, M.-N. Collomb, J. Pécaut, A. Deronzier and F. Neese, *Chem. Eur. J.*, 2008, **14**, 6498-6509.
68. C. Duboc, D. Ganyushin, K. Sivalingam, M. N. Collomb and F. Neese, *J. Phys. Chem. A*, 2010, **114**, 10750-10758.
69. S. Zein, C. Duboc, W. Lubitz and F. Neese, *Inorg. Chem.*, 2008, **47**, 134-142.
70. S. Romain, C. Duboc, F. Neese, E. Rivière, L. R. Hanton, A. G. Blackman, C. Philouze, J.-C. Leprêtre, A. Deronzier and M.-N. Collomb, *Chem. Eur. J.*, 2009, **15**, 980-988.
71. Y. Umena, K. Kawakami, J. R. Shen and N. Kamiya, *Nature*, 2011, **473**, 55-U65.
72. X. Zeng, D. Coquiere, A. Alenda, E. Garrier, T. Prange, Y. Li, O. Reinaud and I. Jabin, *Chemistry-a European Journal*, 2006, **12**, 6393-6402.
73. L. Palatinus and G. Chapuis, *J. Appl. Cryst.*, 2007, **40**, 786-790.
74. O. V. Dolomanov, L. J. Bourhis, R. J. Gildea, J. A. K. Howard and H. Puschmann, *J. Appl. Crystallogr.*, 2009, **42**, 339-341.
75. S. Stoll and A. Schweiger, *J. Magn. Reson.*, 2006, **178**, 42-55.
76. F. Neese, *Wiley Interdiscip. Rev. Comput. Mol. Sci.*, 2012, **2**, 73-78.
77. S. Zein and F. Neese, *J. Phys. Chem. A*, 2008, **112**, 7976-7983.
78. Q. Scheifele, C. Riplinger, F. Neese, H. Weihe, A. L. Barra, F. Juranyi, A. Podlesnyak and P. L. W. Tregenna-Piggott, *Inorg. Chem.*, 2008, **47**, 439-447.
79. J. M. Tao, J. P. Perdew, V. N. Staroverov and G. E. Scuseria, *Phys. Rev. Lett.*, 2003, **91**.
80. F. Weigend and R. Ahlrichs, *Phys. Chem. Chem. Phys.*, 2005, **7**, 3297-3305.
81. F. Weigend, *Phys. Chem. Chem. Phys.*, 2006, **8**, 1057-1065.
82. T. Lu and F. Chen, *J. Comput. Chem.*, 2012, **33**, 580-592.
83. W. Humphrey, A. Dalke and K. Schulten, *Journal of Molecular Graphics & Modelling*, 1996, **14**, 33-38.
84. M. Bühl, C. Reimann, D. A. Pantazis, T. Bredow and F. Neese, *Journal of Chemical Theory and Computation*, 2008, **4**, 1449-1459.
85. A. D. Becke, *Physical Review A*, 1988, **38**, 3098-3100.
86. J. P. Perdew, *Physical Review B*, 1986, **33**, 8822-8824.
87. A. Schäfer, C. Huber and R. Ahlrichs, *The Journal of Chemical Physics*, 1994, **100**, 5829-5835.